Research Square

Preprints are preliminary reports that have not undergone peer review.
They should not be considered conclusive, used to inform clinical practice,
or referenced by the media as validated information.

Assessing reservoir water level and volume based on satellite products: a Portuguese case study

I. Cardenas

icardenas@ciimar.up.pt

University of Porto

A.M. Bento

CIIMAR/CIMAR LA, University of Porto

M. Costa

University of Porto

A. Bio

CIIMAR/CIMAR LA, University of Porto

Research Article

Keywords: Remote sensing, Reservoir monitoring, Water volume estimation, Sentinel–1 SAR, Normalized Difference Water Index (NDWI), Digital Elevation Model (DEM).

Posted Date: November 17th, 2026

DOI: https://doi.org/10.21203/rs.3.rs-11455944/v1

License: This work is licensed under a Creative Commons Attribution 4.0 International License.
Read Full License

Additional Declarations: No competing interests reported.

Assessing reservoir water level and volume based on satellite products: a Portuguese case study

Cardenas, I.[1,2], Bento, A.M.[2,3], Costa, M.[3,2], Bio, A.[2,1]

[1] Department of Biology, Faculty of Sciences, University of Porto, 4169–007 Porto, Portugal

[2] CIIMAR/CIMAR LA, Interdisciplinary Centre of Marine and Environmental Research, University of Porto, Matosinhos, Portugal

[3] Department of Civil Engineering and Georesources, Faculty of Engineering, University of Porto, Porto, Portugal

ORCID:

Cardenas, I. https://orcid.org/0000–0002–8620–3321, Bento, A.M. https://orcid.org/0000–0002–8386–807X, Costa, M. https://orcid.org/0000–0002–4486–7656, Bio, A. https://orcid.org/0000–0003–4501–9410

Correspondence: icardenas@ciimar.up.pt

Abstract

Monitoring reservoir storage dynamics is critical for effective water resource management. The present study evaluates the accuracy of satellite–derived water surface areas, levels, and volumes by comparing them against a Digital Elevation Model (DEM) reference baseline derived from a 2025 LiDAR survey. Water masks were extracted using optical indices (Normalized Difference Water Index from Sentinel-2 and Landsat 8/9) and Synthetic Aperture Radar (SAR) backscatter data (Sentinel–1 VV polarization). The volume estimates derived from satellite data demonstrated a high degree of consistency with DEM references, with differences ranging from –4.4% to –0.3%. Furthermore, NDWI–based volume–water level regressions yielded R^2 values approaching 1. Conversely, the estimates of water surface area demonstrated considerable variability (–6.0% to 8.0%) and exhibited an unsatisfactory correlation with the measured water levels. A key finding is that substantial discrepancies in shoreline delineation resulted in only minor volumetric differences, indicating that volumetric integration mitigates shoreline classification uncertainties, particularly in shallow littoral zones. In conditions of clear sky, optical indices generally outperform SAR. Nevertheless, SAR remains an indispensable tool for continuous monitoring during periods of cloud cover and low illumination. These findings enhance the understanding of uncertainty propagation from remote sensing water masks to storage estimates, providing a more decision–relevant framework for reservoir monitoring methodologies.

Keywords

Remote sensing, Reservoir monitoring, Water volume estimation, Sentinel–1 SAR, Normalized Difference Water Index (NDWI), Digital Elevation Model (DEM).

1. INTRODUCTION

Reservoirs represent pivotal elements within the domain of water–resource systems, serving the critical function of supplying water for various purposes. These include domestic consumption, irrigation, hydropower generation, and flood mitigation. The importance of these water bodies has increased significantly in recent decades due to climate variability, recurrent droughts, and growing water demands, which are placing increasing pressure on freshwater resources worldwide. In such circumstances, precise data concerning reservoir storage is imperative for the effective planning of water resources, the effective management of operations, the generation of energy, and the adaptation to a changing climate. This is because stored water signifies the capacity of a system to

equilibrate temporal discrepancies between water availability and demand (Damkjaer and Taylor 2017; Rodell et al. 2018; Scanlon et al. 2023).

The efficacy of reservoir management is contingent upon the continuous observation of water levels, the extent of water bodies, and the total volume of water stored. Conventionally, the monitoring of these variables has been conducted through in–situ hydrological and hydrometric networks. However, gauging stations are often distributed unevenly, expensive to maintain, and unavailable in many regions of the world. Furthermore, the density of monitoring networks has declined in several countries, limiting the availability of long–term and spatially representative observations of inland waters (Crétaux and Birkett 2006; Schwatke et al. 2015; Kossieris et al. 2024). These limitations are of particular significance for small and medium–sized reservoirs, which frequently lack comprehensive monitoring despite their importance for local water security. Consequently, satellite remote sensing has become an increasingly important source of information for inland–water monitoring, providing regular, large–scale observations over data–scarce and inaccessible regions (Busker et al. 2019; Donchyts et al. 2022; Cretaux et al. 2023).

The remote sensing of inland waters has evolved considerably over the past two decades. While early studies primarily focused on mapping the extent of the water surface, contemporary approaches increasingly seek to estimate changes in reservoir storage by integrating information on water extent, water level and topography. This shift reflects the recognition that storage is a more meaningful hydrological variable than surface area alone since reservoir operation, drought assessment and water–allocation decisions ultimately depend on water volume rather than inundated area (Busker et al. 2019; Li et al. 2021; Chen et al. 2024). Recent advances therefore emphasise integrated monitoring frameworks capable of linking water surface observations with topographic information to quantify storage dynamics across multiple spatial and temporal scales.

Among the available data sources, optical multispectral imagery acquired by Landsat and Sentinel satellites is one of the most widely used methods for mapping surface water due to its long historical archive, global coverage and moderate–to–high spatial resolution (Schwatke et al. 2019; Hou et al. 2024). Water extraction is commonly based on spectral indices, particularly the Normalised Difference Water Index (NDWI), which was introduced by McFeeters (1996) and enhances open water features while suppressing the influence of vegetation and soil backgrounds. Subsequent developments, including the modified NDWI (MNDWI), have improved the discrimination of water from built–up areas under complex land cover conditions (Xu 2006). However, optical approaches are still sensitive to cloud cover, atmospheric effects, mixed pixels and shoreline complexity. These factors can introduce uncertainty when delineating water boundaries (Huang et al. 2018; Donchyts et al. 2022).

Synthetic Aperture Radar (SAR) imagery is a significant complement to optical observations due to its capacity to function independently of cloud cover and illumination conditions. Consequently, Sentinel–1 SAR data has become extensively utilised in operational reservoir and flood–monitoring applications, particularly in scenarios where cloud–free optical imagery is scarce (Souza et al. 2022; Tottrup et al. 2022). However, the accuracy of SAR–derived water maps is contingent on numerous factors, including uncertainty associated with vegetation cover, shoreline morphology, soil moisture, and surface roughness, which renders their classification performance dependent on local environmental conditions (Souza et al. 2022; Declaro and Kanae 2024). Consequently, contemporary state–of–the–art monitoring systems are increasingly reliant on the complementary utilisation of optical and SAR observations, as opposed to reliance on a singular sensor.

Recent advancements have demonstrated that combining satellite–derived water extent with Digital Elevation Models (DEMs), bathymetric information, and water–level observations enables the construction of area–elevation–volume (AEV) relationships and the estimation of reservoir storage

dynamics at local, regional, and global scales (Busker et al., 2018; Liu et al., 2020; Li et al., 2021). These approaches have proven particularly valuable in ungauged or poorly monitored regions, where conventional observations are unavailable or incomplete (Avisse et al., 2017; Getirana et al., 2018; Chen et al., 2024). However, the accuracy of these models is dependent on several factors, including the morphology of the reservoir, the complexity of the shoreline, the quality of the Digital Elevation Model (DEM), and the extent to which basin topography was exposed at the time of DEM acquisition (Avisse et al., 2017; Ahmed et al., 2025; Lima et al., 2025).

Despite considerable advances in satellite–based reservoir monitoring, most studies evaluate sensor performance primarily in terms of the accuracy of water–surface delineation. However, from a water–management perspective, the principal variable of interest is reservoir storage as opposed to surface area alone. Consequently, a key unresolved question is whether uncertainties associated with shoreline delineation propagate proportionally into estimates of water level and stored volume, or whether basin morphology and hypsometric characteristics damp these errors during volumetric calculations. Whilst some studies suggest that storage estimates may be considerably more robust than area estimates, this phenomenon remains insufficiently quantified, particularly in the context of medium–sized reservoirs and multisensor monitoring frameworks (Avisse et al., 2017; Li et al., 2021; Chen et al., 2024). This issue is of pertinence, given that the operational usefulness of remote–sensing products is contingent on their capacity to provide reliable storage estimates as opposed to merely accurate water masks.

The pertinence of this challenge is especially apparent in Mediterranean regions such as Portugal, where water availability demonstrates marked seasonal variability and rising drought frequency exerts further pressure on reservoir systems. It is therefore imperative to enhance the reliability of storage estimation methods to support water allocation, hydropower production, and drought–management strategies in the context of changing hydroclimatic conditions.

Considering the context, the present study undertakes an evaluation of the performance of Sentinel-2, Landsat 8/9, and Sentinel–1 imagery in the estimation of water extent, water level, and stored volume in the Torrão Reservoir, located in the northern region of Portugal. The satellite–derived products are then compared with reference values obtained from in situ water–level measurements and a high–resolution topo–bathymetric digital elevation model (DEM). This study does not concentrate exclusively on the accuracy of water–surface delineation; rather, it investigates the propagation of sensor–dependent uncertainties in shoreline extraction into estimates of water level and storage. It therefore contributes to a central question in contemporary reservoir monitoring, namely whether integrated satellite–based approaches can provide robust storage estimates despite imperfections in water–boundary detection. To this end, the relationship between classification uncertainty and volumetric estimation is examined. It is anticipated that the findings will contribute to the advancement of multisensory remote–sensing methodologies for operational reservoir monitoring and water–resource management.

2. STUDY AREA

2.1 Study Area Description

The Torrão Reservoir lies in northern Portugal on the Tâmega River, a major right–bank tributary of the Douro River (see Figure 1). The Tâmega catchment encompasses an approximate area of 3,310 km^2, of which about 2,637 km^2 (equivalent to around 80%) are situated within Portuguese territory. The river extends for a total of 184.02 km and exhibits an average annual discharge of 70.31 m^3s^{-1}. The land use within the basin is dominated by forests and semi–natural areas (60.6%) and agricultural

land (37.6%), whereas artificial surfaces represent a mere 1.5% of the total catchment area, thereby reflecting the predominantly rural character of the basin (Agência Portuguesa do Ambiente 2020).

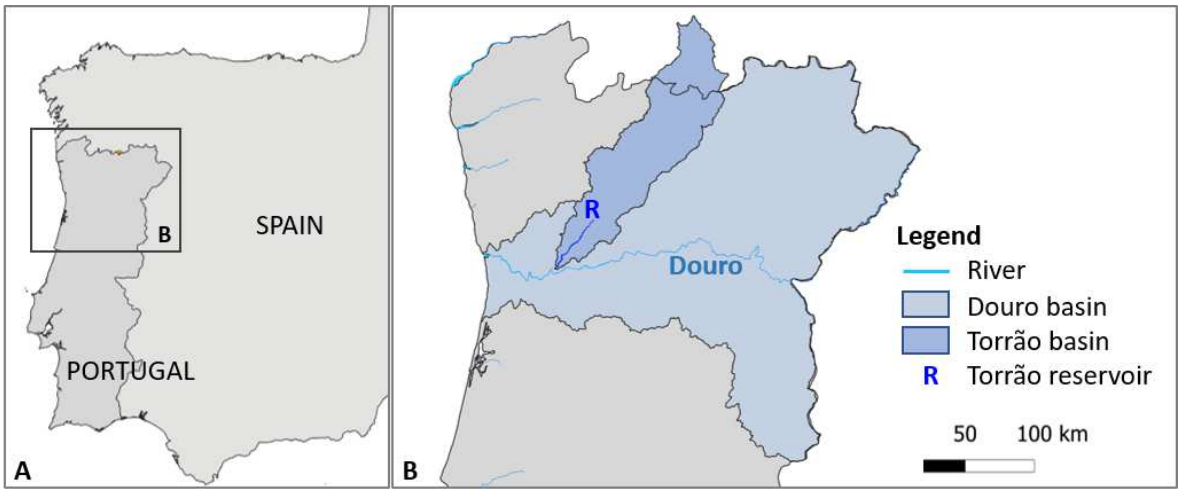


Figure 1. Overview of the location of the study area in northern Portugal (A) and location of the Tâmega and Douro basins and the Torrão reservoir (B).

The construction of the Torrão Dam, in 1988, was undertaken for the purpose of hydropower generation, thus playing a pivotal role in the effective management of water resources within the confines of the Douro basin (Agência Portuguesa do Ambiente 2025). The reservoir exhibits notable seasonal and interannual fluctuations in water level, inundated area, and storage volume, reflecting both natural hydrological variability and operational management requirements. These variations render the reservoir particularly well–suited for the evaluation of remote sensing approaches for the estimation of water extent, water level, and stored volume.

From a geomorphological perspective, the reservoir displays an elongated shape, characterised by multiple tributary branches and shoreline sections exhibiting variable topography (Agência Portuguesa do Ambiente 2025). Such characteristics are of relevance to remote sensing applications, given that the complexity of shorelines and the local terrain conditions directly influence the accuracy of water–surface delineation. Consequently, the Torrão Reservoir provides an appropriate setting for investigating the effects of sensor–dependent uncertainties on storage estimation.

Moreover, the availability of high–resolution topographical and bathymetric information, as well as historical water–level observations, provides a valuable reference dataset for validating satellite–derived estimates. These characteristics render the Torrão Reservoir a representative medium–sized reservoir, where reliable monitoring of water storage is imperative for operational management, though continuous field observations may not always be feasible.

2.2 Hydrological Characteristics and Monitoring

The Tâmega River basin is distinguished by pronounced hydrological variability, driven by seasonal precipitation patterns that are characteristic of northern Portugal. High–flow periods have been observed to occur during the wetter months, whereas lower flows are typically observed during the summer season. This variability gives rise to considerable temporal fluctuations in reservoir extent, water level, and storage volume, thus creating a suitable framework for the evaluation of the performance of different satellite–based monitoring approaches.

Historically, hydrological monitoring within the basin has been facilitated by the presence of several gauging stations. A study was conducted in Amarante, located downstream of the Torrão Reservoir, in which water levels were measured through a staff gauge at São Gonçalo over a period of 18 years, from 1937 to 1955. This provided daily observations of river water levels (Tedim and Carvalho 2010). Subsequently, a limnometric station was operated between 1985 and 2001, generating continuous records of water–level variations, although there were some data gaps during periods of equipment malfunction (Tedim and Carvalho 2010). These observations constitute a significant source of information for understanding the hydrological behaviour of the basin and provide valuable context for evaluating remote sensing products.

The lower Tâmega valley, particularly in the urban area of Amarante, has historically been subject to recurrent flood events due to the confluence of three factors: high river discharges, valley confinement, and the local river morphology. Consequently, Amarante has been designated as an Area of Potential Significant Flood Risk (*Área de Risco Potencial Significativo de Inundação*, ARPSI) within the Flood Risk Management Plan for the Douro Hydrographic Region (RH3) (Agência Portuguesa do Ambiente 2025). As demonstrated by historical records, there have been numerous instances of flooding throughout the twentieth and early twenty–first centuries. This underscores the necessity of ongoing hydrological monitoring and the implementation of effective water management strategies within the basin (Tedim and Carvalho 2010).

While flood–risk assessment is not the primary focus of the present study, the hydrological variability observed within the Tâmega basin emphasises the need for accurate and timely information on reservoir state and storage conditions. In this context, satellite remote sensing offers a valuable addition to conventional monitoring networks by providing regular observations of water extent and storage dynamics.

The combination of significant water–level fluctuations, complex shoreline geometry, historical monitoring records, and the availability of a high–resolution topo–bathymetric Digital Elevation Model make the Torrão Reservoir an appropriate case study for evaluating the performance of Sentinel-2, Landsat 8/9, and Sentinel–1 imagery in estimating water extent, water level, and stored volume. Moreover, these characteristics furnish a suitable framework for analysing how uncertainties in water–surface delineation influence the accuracy of reservoir storage estimates.

3. DATA

3.1 Remote sensing data

The analysis drew upon a range of satellite–derived datasets, encompassing optical sensor information from Sentinel-2 (with a resolution of 10 m), along with data from Landsat 8 and 9 (which offer a resolution of 30 m). The study also incorporated Synthetic Aperture Radar (SAR) data from Sentinel–1, with a resolution of 10 m. The selection of data was based on the image quality and data accessibility through the Copernicus program (https://browser.dataspace.copernicus.eu/) and the USGS EarthExplorer (https://earthexplorer.usgs.gov/). To minimize errors in classification associated with cloud contamination, only images with less than 10% cloud cover were considered. The acquisition dates for each source are documented in Table 1.

3.2 *Digital elevation model and bathymetry*

Accurate representation of both terrestrial and submerged topography is imperative for reliable reservoir–scale geomorphological and hydrological analyses. Therefore, a high–quality Digital Terrain Model (DTM) of the Torrão reservoir and its surrounding areas was employed, as well as the most advanced bathymetric data available.

Topographic data for the study area were collected from the Portuguese Directorate–General for Territory (DGT) (DGT 2026) and consisted of a high–resolution DEM with a spatial resolution of 0.5 m, derived from a LiDAR survey with an average density of 10 points/m^2 (Agência Portuguesa do Ambiente 2020). Outside the reservoir boundaries the DGT DEM was used directly. As LiDAR data did not penetrate the water, thus not providing bathymetric data, LiDAR topography was merged with available bathymetry data.

As the Torrão reservoir is located within an Area of Potential Significant Risk of Flooding (ARPSI), namely the Amarante ARPSI, the Portuguese Environment Agency provides flood depth and maximum flood level maps for a 100–year return period (Agência Portuguesa do Ambiente 2020). Hence, the bathymetric data of the Torrão reservoir were estimated by computing the difference between maximum flood levels and corresponding depths. In the area extending 100 m upstream from the dam, no flood information was available. Consequently, the implementation of bathymetric correction was not a viable option, and the original terrain elevation dataset was maintained.

In order to ensure spatial consistency between terrestrial and submerged terrain representations, the bathymetrically corrected surface was resampled to the native 0.5 m resolution of the DGT DEM, with the resulting topo–bathymetric DEM providing a seamless representation of reservoir morphology across both subaerial and submerged areas. Finally, the DEM was clipped using a 200–metre buffer around the Torrão reservoir, thereby defining the study domain for all subsequent analyses.

3.3 In situ water levels

Water levels were obtained from the hydrometric station “Albufeira do Torrão (R.E.)", code SNIRH 07H/01A, located in the proximity to the Torrão dam, for the dates for which adequate–quality satellite data was available (Table 1). Water levels tend to increase up–river. Consequently, the water–level measuring station at the Torrão dam was used to define the study area, with a specific focus on the reservoir segment where water levels remain constant (Figure 2).

Table 1. Dates for which adequate–quality satellite products were available and respective water levels measured at a hydrometric station near the dam (see Figure 2).

Date	Water level (m)	Optical		Radar (SAR)
		Landsat 8/9	Sentinel 2	Sentinel–1
23/02/2017	58.36	X		
24/02/2017	58.44		X	X
29/12/2019	58.98		X	X
30/12/2019	58.28	X		X
04/04/2022	59.94		X	
16/09/2024	60.50			X
07/07/2025	60.20	X	X	X
03/10/2025	58.66	X	X	
05/10/2025	59.33		X	X
12/10/2025	59.25		X	
13/10/2025	58.92		X	

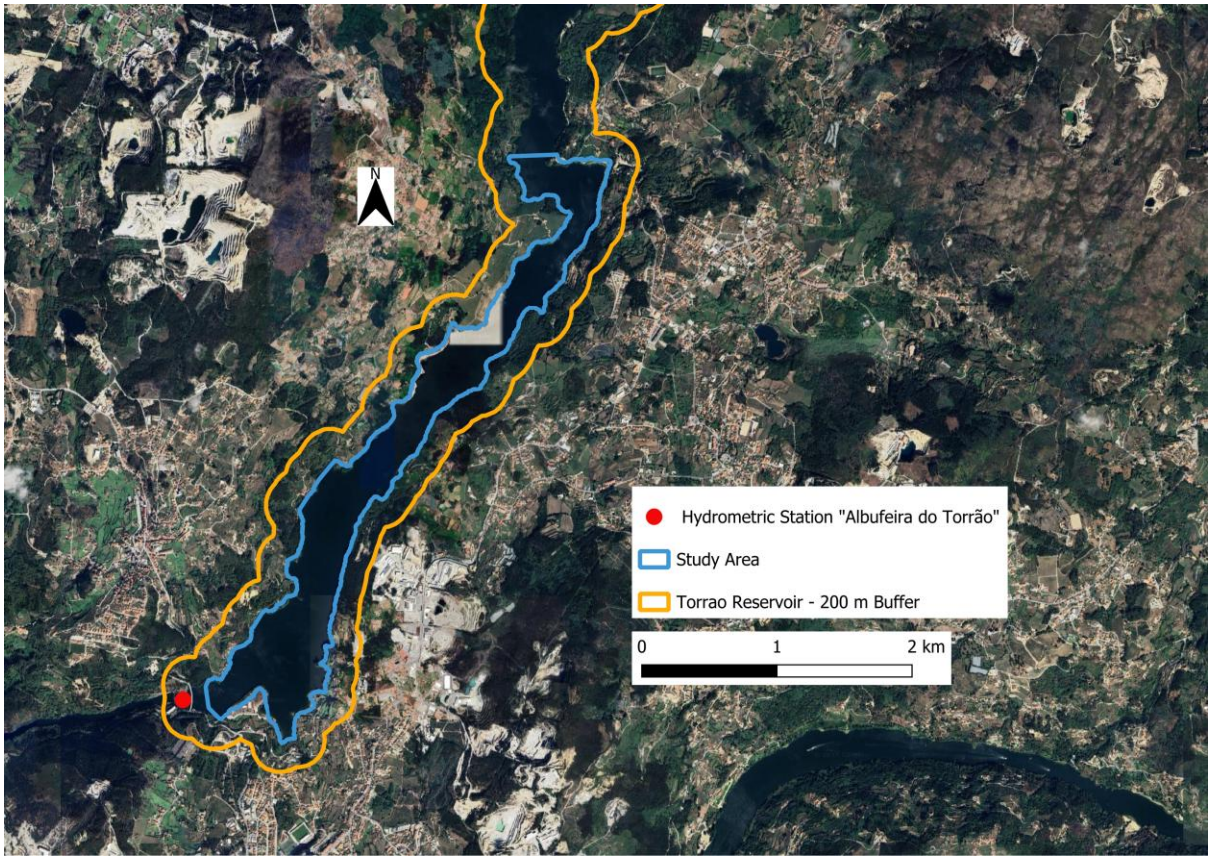


Figure 2. Location of the Hydrometric station Albufeira do Torrão Reservoir in northern Portugal. The blue line delimits the water surface of the reservoir, while the orange line delimits the study area, defined as the reservoir plus a 200 m buffer.

4. METHODS

The methodological framework for estimating water surface areas, levels, and volumes is illustrated in Figure 3. The water surfaces and volumes calculated using the DEM area and volume below the respective measured water levels were considered to be correct, particularly for the 2025 dates (Table 1), which is the year of the LiDAR survey. The results obtained for the various satellite products were then compared with the ones obtained for the DEM (Figure 8). The geographic information was visualized and processed in QGIS (version 3.44.12) using the ETRS89 / Portugal TM06 (EPSG:3763) coordinate reference system.

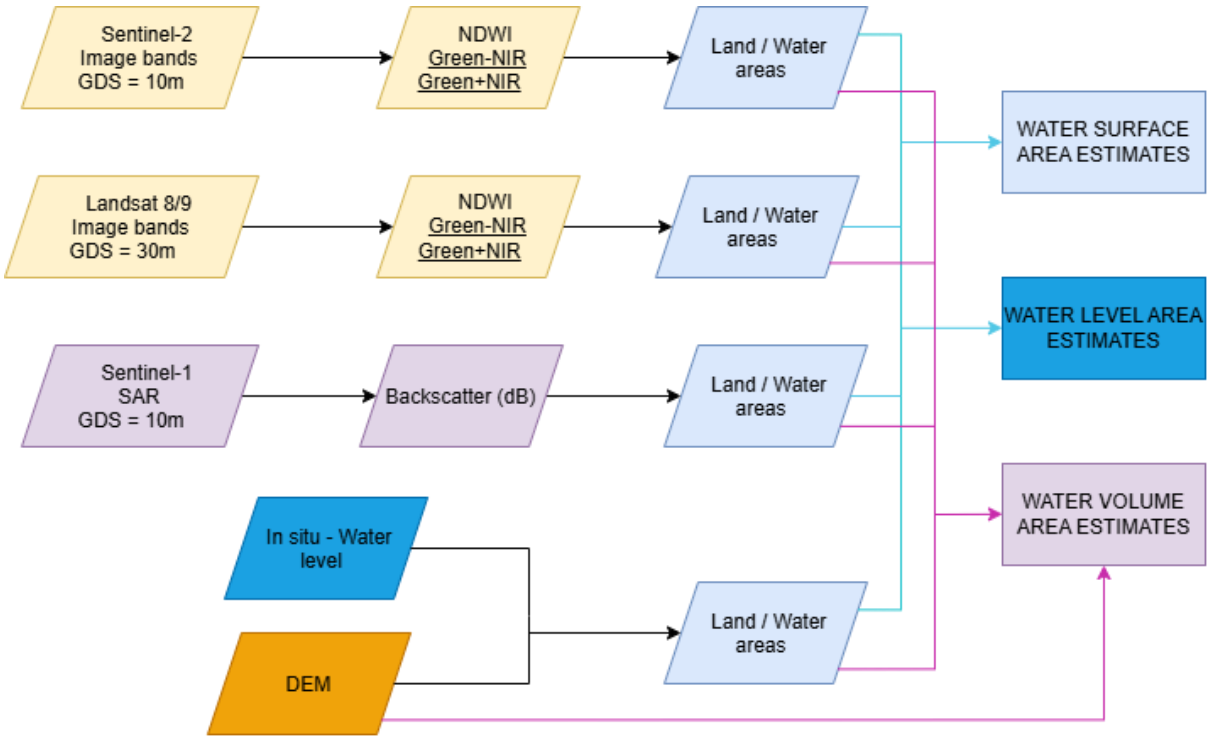


Figure 3. Methodology for water surface, level and volume estimation.

4.1 Water surface extraction from DEM data

Water surface areas for the different survey dates were obtained by extracting the DEM contour lines for the respective in–situ measured water levels. The polygonization of these contours was undertaken for the study area, thus enabling the calculation of the DEM–derived water surface area.

4.2 Water surface extraction from optical data

Sentinel-2 images were acquired from the Copernicus Open Access Hub, while Landsat 8/9 imagery was obtained from the USGS Earth Explorer for the matching acquisition dates (Table 1). The Normalized Difference Water Index (NDWI) was calculated using bands 3 (Green) and 8 (NIR) for Sentinel-2, and bands 3 (Green) and 5 (NIR) for Landsat 8/9. A binary water/non–water mask was then generated by applying thresholds of ≥ –0.2 (for Sentinel 2) and ≥ –0.13 (for Landsat 8/9), determined as described in section 4.4, using the Raster Calculator tool in QGIS. In order to facilitate accurate area calculations, reprojection of both raster layers was conducted to EPSG:3763. The NDWI was computed for both sensors using the standard formulation Eq. (1).

$$NDWI = \frac{\text{Green}+NIR}{\text{Green}-\text{NIR}} \qquad (1)$$

4.3 Water surface extraction from SAR data

Unlike optical sensors, Synthetic Aperture Radar (SAR) is capable of recording the backscatter of a microwave signal emitted by a satellite. The nature of this backscatter is dependent on surface properties such as roughness, moisture, and structure, as well as on the geometry of the sensor. This characteristic renders SAR particularly well–suited for continuous monitoring, as it can operate both diurnally and nocturnally, and in a range of weather conditions (Lekunberri et al. 2024).

The VV polarization was used in this study for water detection purposes, as it has been demonstrated to be sensitive to surface heterogeneity and roughness (Rossi et al. 2023; Lekunberri et al. 2024). It is

a widely adopted technique in environmental monitoring applications, including threshold–based segmentation of water bodies and tracking of river dynamics during extreme events (Rossi et al. 2023).

Sentinel–1 Level 1 GRD COG images were selected from the Copernicus Explorer portal for the same dates as the optical images. The processing of the data was carried out using ESA's SNAP (Sentinel Application Platform) software, an open–source toolbox that that facilitates the automated preprocessing of SAR data in accordance with standard workflows (Filipponi 2019; Lekunberri et al. 2024).

The pre–processing chain comprised the following steps: the application of precise orbit files to improve satellite position and velocity information; the removal of thermal noise, which is especially important for the cross polarisation channel; radiometric calibration, which ensures that pixel values are proportional to radar backscatter and enables comparison across different acquisitions; speckle filtering using a Lee filter to reduce the granular noise inherent to SAR imagery while preserving edges and fine details; and terrain correction to compensate for geometric distortions caused by topography and satellite tilt (Figure 4), which also geocodes the image (Filipponi 2019).

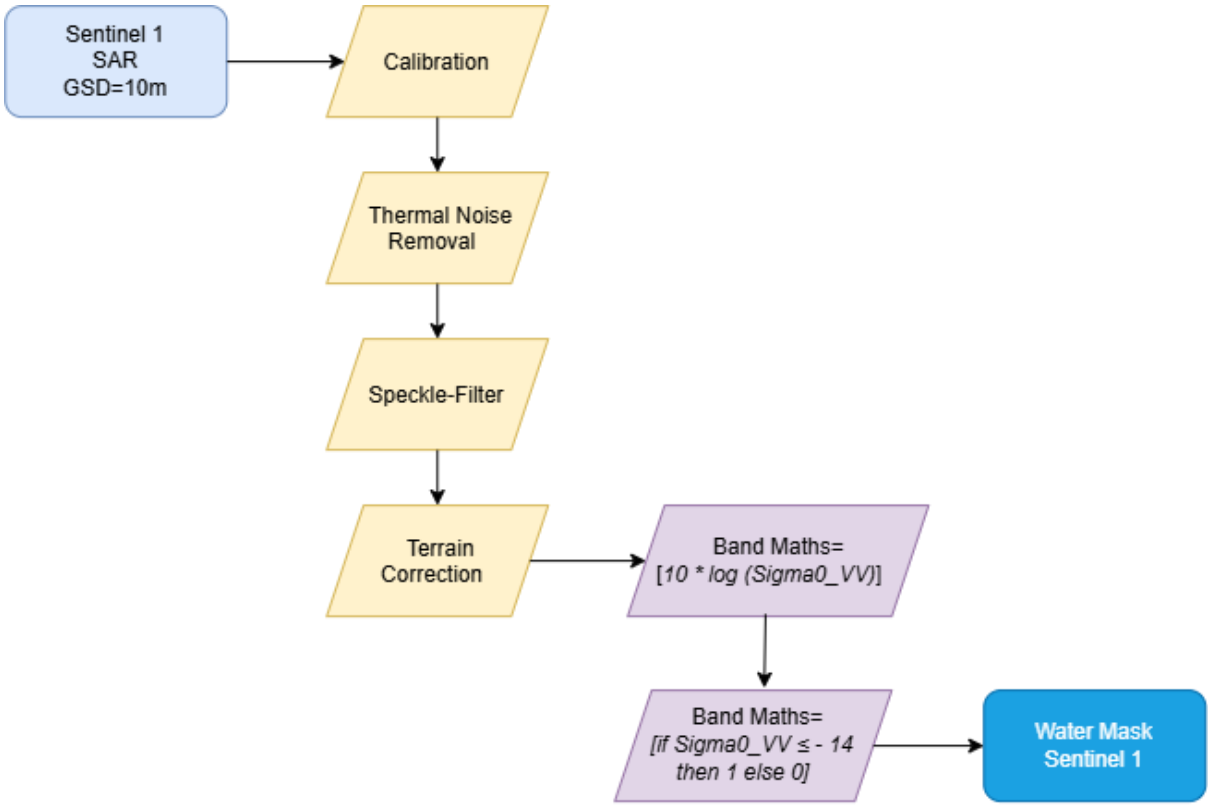


Figure 4. Processing the configuration of Sentinel–1 products in SNAP.

After pre–processing, a band-math operation was applied to convert the calibrated backscatter values (Sigma0) to decibels (dB) (Fikriyah et al. 2025) using Eq. (2).

$$\sigma\mathrm{VV,dB} = 10\,log(\sigma\mathrm{VV}) \qquad (2)$$

Conversion to decibels (dB) is essential as it compresses the broad dynamic range of SAR backscatter values, which can vary by several orders of magnitude, into a more manageable logarithmic scale (Roßberg and Schmitt 2025). This scale also renders the data distribution more Gaussian (Goodman 1963), a development which is of benefit to statistical analysis and thresholding, and which aligns more closely with human visual perception, thus facilitating image interpretation. Furthermore, it

follows the standard practice of defining many empirical thresholds in dB (Dunmire et al. 2024). The representation of backscatter in decibels constitutes a standard practice in the analysis of Sentinel–1 data, as evidenced by the utilization of cross–polarization ratio (VH–VV; in dB) in addition to cross–polarization alone. This approach assists in mitigating the impacts of ground, vegetation, and surface geometry properties (Dunmire et al. 2024). Radiometric calibration, an essential requirement for conversion, has been thoroughly validated across a wide range of backscatter, ensuring the absolute calibration and consistency of the radar backscatter measured for the Sentinel–1 satellite constellation (Schmidt et al. 2020)

In conclusion, employing the previously determined threshold of –14 dB to differentiate between land and water (see Section 4.4), a binary water mask was generated in SNAP by segmenting the calibrated backscatter raster. Pixels with values below this threshold were classified as water, while those above were classified as land. The binary mask was subsequently reprojected to the national coordinate system (EPSG:3763) and utilized to calculate the area covered by water.

4.4 Threshold determination

To delineate the water–covered area in the satellite products, it was necessary to establish land–water thresholds. Given that the DEM provides contour lines that correspond to the correct water levels for the study area, and that the DEM remains largely unchanged during 2025, satellite products from 2025 were used to assess the NDWI and sigma values that correspond to the limit between dry land and water. The analysis incorporated Sentinel–1 and 2 data from 7th July, 2025, and October 5, 2025, complemented by a Landsat 9 image from October 3, 2025, the closest available alternative for the latter date, as the USGS did not provide an image from that date not obscured by cloud cover.

Two methodologies were employed. The first stage of the research involved the drawing of NDWI and Sigma profiles over a large body of water, with the aim of assessing where the values suddenly change between the land and water surfaces; these profiles were drawn across the lower reservoir, as illustrated in Figure 5.

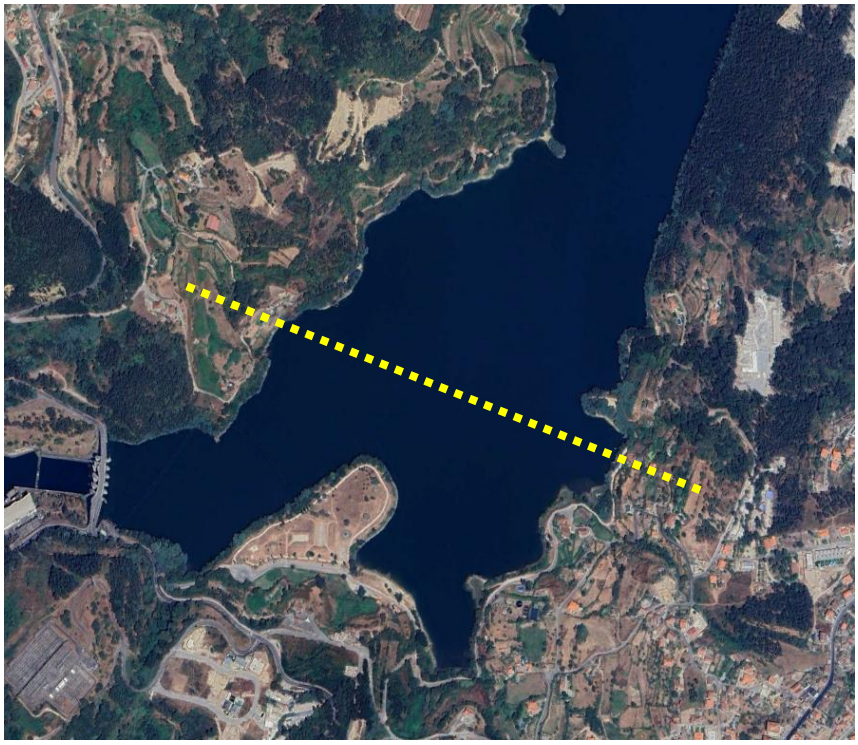


Figure 5. Image of the lower reservoir (source: GoogleEarth, Airbus 2025) with the location of the profiles (yellow dashed line).

The second method involved the extraction of values for the various satellite products along the DEM–derived water limit, with 200 points being drawn along the water–level DEM contour line. The process was executed in QGIS using the "Random points along line" tool, configured to generate points with a minimum distance of 10 meters between points to ensure an even distribution along the water boundary. For each of these points, NDWI and SAR backscatter values were extracted from the 2025 datasets. The mean and standard deviation of the NDWI and SAR backscatter values along the water–level contour line were subsequently calculated and compared to the in–situ measured water levels. This statistical comparison provides an assessment of the correspondence between our NDWI and SAR–backscatter thresholds and the DTM–based water level, as well as an evaluation of the positional correspondence between the estimated water limits. This approach is consistent with established practices for validating optical and SAR–derived water lines using topographic reference data, where intersection with a DEM provides an independent validation of the extracted water boundaries (Musa et al. 2015).

4.5 Water surface and volume estimation

The water masks obtained by employing the DEM water–level contour line and by binarizing the satellite products according to the established threshold values were subsequently polygonised and cut to the study area, and the areas of the resulting polygons were calculated, representing the water–surface areas estimated for each data source. The volume of water contained within the reservoir was estimated by means of the QGIS Volume Calculation Tool plugin. This involved calculating the volume below the respective water level, for the DEM, within the respective water–area polygon. A conventional water area and volume calculation, for all survey data (Table 1), based on the DEM–derived water area polygon, but employing an irregular mesh to calculate areas and volumes, yielded highly comparable values, with RMS differences of 0.006 ha for the area estimates and a RMSE of 0.009 hm^3 for the volumes.

4.6 Water level estimation

To estimate water levels based on the DEM and the satellite products, the vertices of the respective water polygons were extracted to create a point layer. In the case of the Landsat water masks, all vertices along the water–body margins were considered (i.e. approximately 300 to 400). The Sentinel–1 and 2 water–mask rasters resulted in a total of about 1300 vertices, and derived points, while the DEM resulted in more than 25,000 vertices/points. Therefore, 1,000 vertices were randomly selected to extract and analyse the underlying DEM values, with the mean and median values being used as water–level estimates.

5. RESULTS

5.1 Threshold Selection Results

Optimal segmentation thresholds were determined to distinguish water from non–aquatic surfaces using datasets from 7th July and October 3 and 5, 2025, based on the profiles crossing the reservoir near the dam (Figures 2 and 5) and based on the mean NDWI and Sigma values along the DEM–derived water line.

Cross–sectional profiles across the lower reservoir (Figure 6) were analysed for elevation, NDWI, and SAR backscatter. As illustrated in Figure 6a, the digital elevation model (DEM) reveals the elevation profile along the transect, with the valley floor situated between approximately 250 m and 875 m, where elevations decline to 20–40 m above sea level. The in–situ water level on 7th July 2025 (60.20 m) is well above the valley floor, confirming the complete flooding of the central section.

Figure 6b provides a comparison of the Sentinel-2 and Landsat 8 NDWI profiles for the 7th of July 2025. Both sensors produced similar patterns, with NDWI values of up to approximately 0.2 recorded over the water body and falling to near zero or negative values over land. On 5th October 2025 (Sentinel-2, Figure 6c) and 3rd October 2025 (Landsat 9, Figure 6d), the NDWI values over the water were lower (0.06–0.25) than in July, and the apparent width of the water was slightly reduced. The lower resolution of Landsat (30 m) resulted in smoother transitions at the water's edges.

As demonstrated in Figures 6e and 6f, the SAR backscatter profiles exhibit a pronounced contrast between the water and the land. On 7th 7th July, 2025, backscatter over the reservoir ranged from –20 dB to –13 dB. On 5th October 2025, backscatter values over the water were found to be elevated (ranging from –14 dB to –12 dB), while the surrounding land exhibited values above –8 dB. This increase may be attributed to a lower water level, increased surface roughness due to wind, or changes in the sensor geometry.

The NDWI and Sigma values along the DEM–derived waterline (Figure 5) demonstrated some variation (see the Standard Deviation (SD) shown in Table 2), but their mean values correspond to the established land–water limits observed in the respective profiles (Table 2, Figure 6).

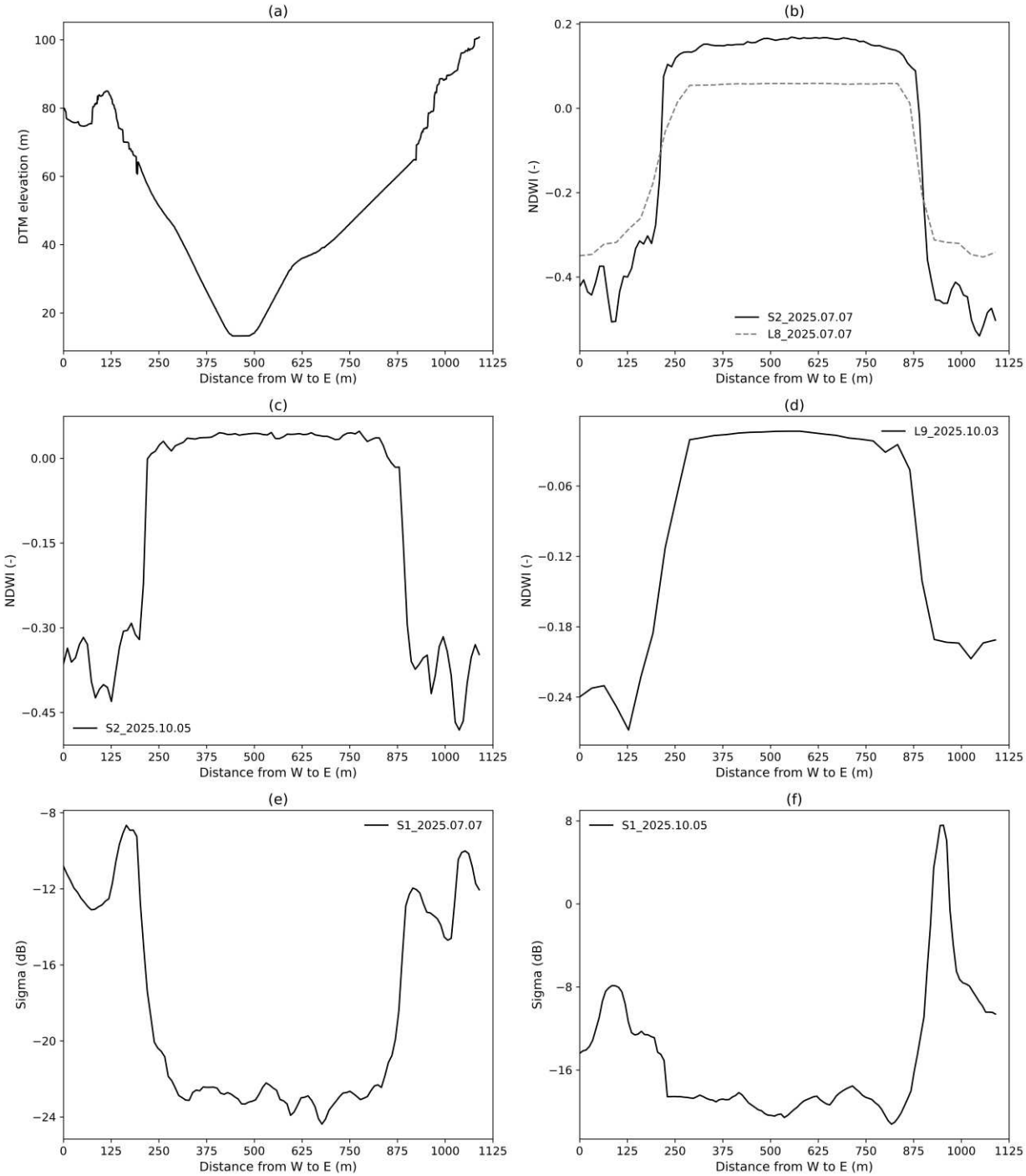


Figure 6. Profiles crossing the reservoir close to the dam (see Fig. 5), for DTM (a), Landsat 8 and Sentinel 2 in July, NWDI (b), Sentinel 2 in October, NWDI (c), Landsat 9 in October, NDWI (d) and the Sentinel–1 SAR (e).

The spatial distribution of NDWI and SAR backscatter values, together with the resulting water/land classifications, is shown in Figure 7 for July and October 2025.

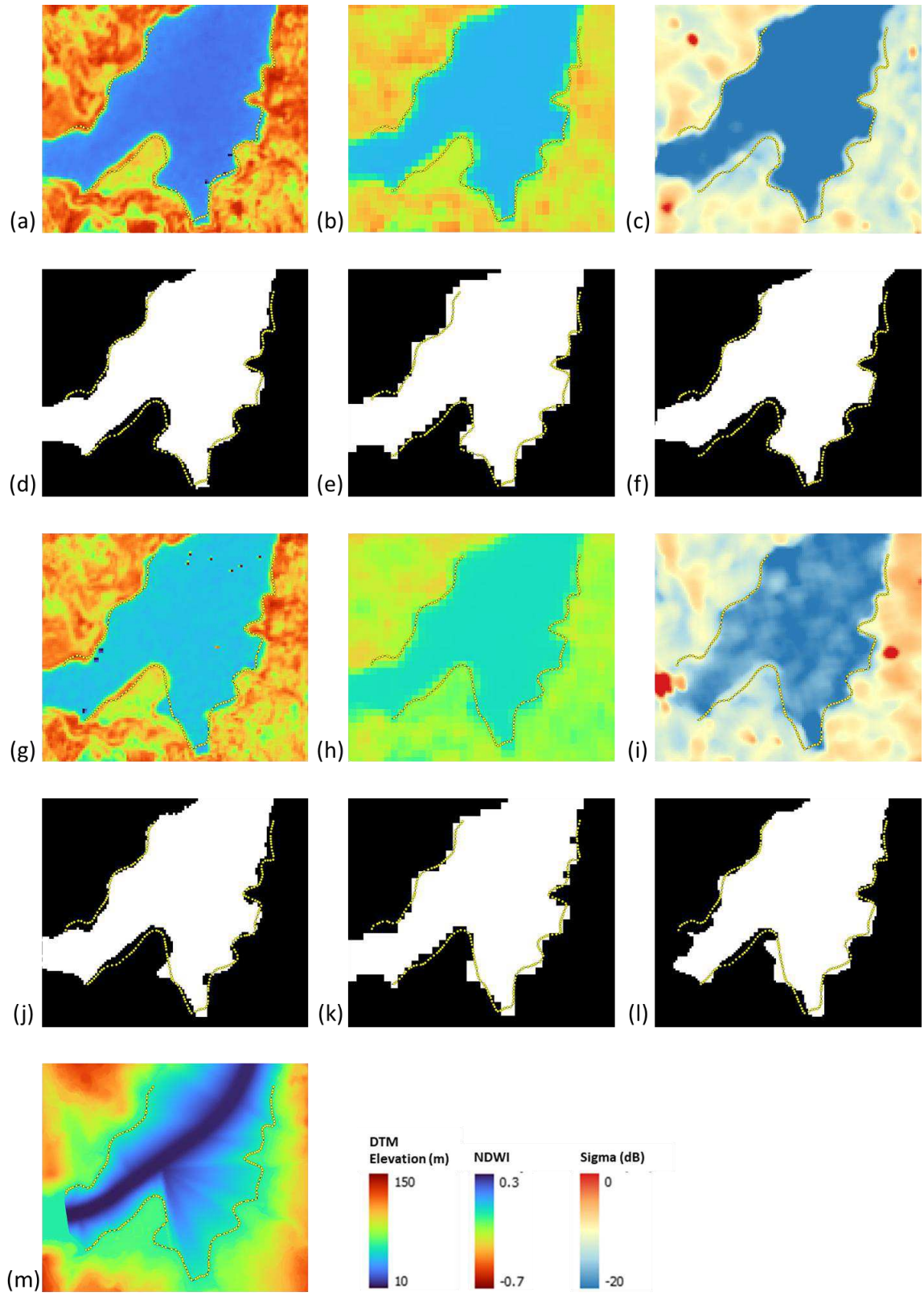


Figure 7. Lower–reservoir maps: Sentinel 2 NDWI (a), Landsat 8 NDWI (b), Sentinel–1 Sigma (c), and water (white)/land (black) classification for Sentinel 2 NDWI (d), Landsat 8 NDWI (e), Sentinel–1 Sigma (f), the DTM (m), for July 2025; Sentinel 2 NDWI (g), Landsat 8 NDWI (h), Sentinel–1 Sigma (i), and water (white)/land (black) classification for Sentinel 2 NDWI (j), Landsat 8 NDWI (k), Sentinel–1 Sigma (l), for October 2025; and, the DTM (m), for spring 2025; all with the respective DTM–based water line and the points used for land–water threshold determination.

Table 2. Mean (SD) values for the DTM and the satellite–data, extracted at the points drawn along the respective waterline (Figure 5) based on the water level measured at the dam, and the respective threshold values selected according to the reservoir–crossing profiles (Figure 6).

Date	Mean (SD)			
	DTM elevation (m MSL)	Sentinel 2 NDWI	Landsat NDWI	Sentinel–1 Sigma (dB)
07 July 2025	60.23 (0.39)	–0.20 (0.20)	–0.15 (0.10)[a]	–13.65 (2.43)
03 October 2025	58.64 (0.46)		–0.11 (0.06)[b]	
05 October 2025	59.27 (0.57)	–0.20 (0.17)		–14.50 (2.80)
Threshold		–0.20	–0.13	–14.00

[a] Landsat 8
[b] Landsat 9

For optical indices, an upper threshold of –0.2 was established for the Normalized Difference Water Index (NDWI) derived from Sentinel-2 and of –0.13 for the NDWI from Landsat 8 images. For SAR backscatter (Sentinel–1, VV polarization), a threshold of –14 dB was applied. These thresholds were used for the subsequent generation of the water masks and the calculation of areas.

5.2 Comparison of estimated water–covered areas and water volumes

The water masks generated using the three data types (Sentinel-2 and Landsat 8 and 9 NDWI and Sentinel–1 SAR backscatter) were compared for the study area. Visual inspection of the satellite–derived water extents revealed a general consistency, although some discrepancies were observed (Figure 8). The satellite–based masks exhibited discrepancies from the reference waterline derived from the DEM, particularly at the reservoir margins and in areas of very shallow water.

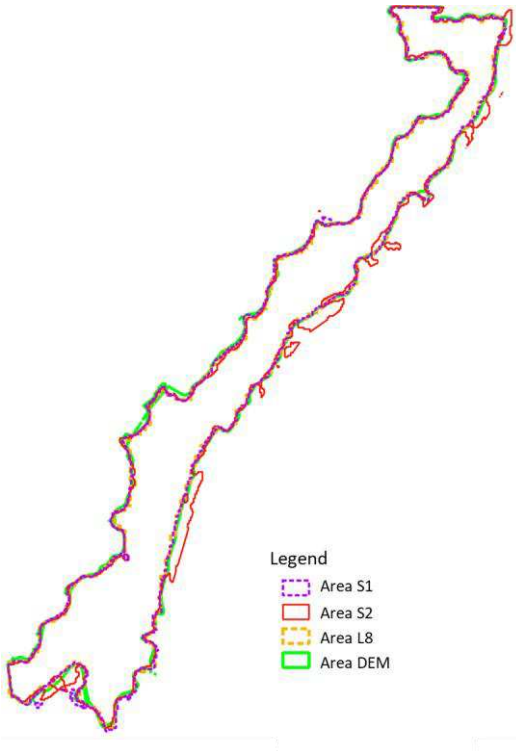


Figure 8. Water polygons obtained using the DEM, Landsat 8 and Sentinel 2 satellite NDWI and Sentinel–1 Sigma, for 7th July 2025.

The areas of satellite water masks vary markedly (Table 3, Figure 7), showing little relation to the respective water levels (Figure 9). This indicates that higher water levels do not necessarily correspond to larger estimated water areas.

The water level estimates demonstrate a comparable pattern, with satellite–derived estimates frequently exhibiting significant over– or under–estimation of the reference water level. Table 4 presents the comparison for the DEM and Landsat 8/9, while Table 5 presents the results for Sentinel-2 and Sentinel–1 (Figure 10). The median of the estimated values demonstrates superior performance in comparison to the mean. The ranges indicate that the water mask crosses pixels of very different DEM heights. The various extents of the water masks (Figure 8) suggest that the Sentinel-2 NDWI is particularly effective in identifying areas of higher elevation as water. Nonetheless, the analysis of the Landsat and Sentinel–1 products indicated the most significant variability in water–level estimates. The DEM–derived water level demonstrates the greatest efficacy, as would be anticipated, given that the estimation method is based on DEM contour lines. The minor discrepancies observed between the DEM estimates and the in–situ measurements can be attributed to errors introduced during the data processing phase, including the projection of the satellite image coordinate system to ETRS and the conversion of raster to polygon formats. These errors may have been exacerbated by the inclination of the terrain. However, these errors are negligible, ranging from −7 cm to +9 cm for the mean and from 0 cm to 2 cm for the median estimated water levels. Landsat demonstrated the poorest performance, with differences ranging from −3.24 m to +5.54 m for the mean and from −1.88 m to 2.67 m for the median estimated water levels. Sentinel-2 revealed variations in water levels ranging from −2.18 m to +3.09 m for the mean and from −1.48 m to +1.89 m for the median. For Sentinel–1, the differences in water level measurements varied between −2.18 m and +2.64 m for the mean and between −1.48 m and +1.27 m for the median.

Conversely, volumes exhibited a strong correlation with the reference DEM volumes, albeit consistently lower, and demonstrated a consistent alignment with water levels, with higher levels corresponding to larger volumes (Table 6, Figure 11). Linear regression models of the NDWI–based volumes in relation to water level exhibited R^2 values close to 1, similar to the DEM–based results. The Sigma–based volume estimates demonstrate slightly lower performance (R^2 = 0.922).

Table 3. Water–covered areas calculated using the DEM and the different satellite products, and % difference (Diff.) between each satellite result and the reference DEM result.

Date	In–situ water level (m)	Water–covered area (ha)						
		DEM	Landsat 8/9	Diff.	Sentinel 2	Diff.	Sentinel–1	Diff.
23/02/2017	58.36	167.52	174.02	+3.9%				
24/02/2017	58.44	167.83			177.27	+5.6%	165.17	−1.6%
29/12/2019	58.98	169.89			176.75	+4.0%	161.54	−4.9%
30/12/2019	58.28	167.22	180.52	+8.0%			175.44	+4.9%
04/04/2022	59.94	173.66			173.82	+0.1%		
16/09/2024	60.50	177.59					166.85	−6.0%
07/07/2025	60.20	176.01	167.33	−4.9%	170.96	−2.9%	177.36	+0.8%
03/10/2025	58.66	168.67	163.22	−3.2%	169.84	+0.7%		
05/10/2025	59.33	171.24			168.06	−1.9%	175.08	+2.2%
12/10/2025	59.25	170.93			170.07	−0.5%		
13/10/2025	58.92	169.66			170.76	+0.6%		

Table 4. In–situ measured water levels compared to estimated water levels using the DEM and Landsat 8/9.

Water level (m)							
Date	In–situ water level (m)	DEM			Landsat 8/9		
		Mean (Min–Max)	SD	Median	Mean (Min–Max)	SD	Median
23/02/2017	58.36	58.33 (55.80–58.93)	0.34	58.36	59.05 (25.51–105.87)	11.77	58.66
24/02/2017	58.44	58.38 (55.80–59.01)	0.40	58.44			
29/12/2019	58.98	58.93 (55.85–61.68)	0.43	58.98			
30/12/2019	58.28	58.25 (55.71–58.82)	0.34	58.30	63.82 (20.21–107.27)	17.05	60.95
04/04/2022	59.94	59.86 (55.81–63.57)	0.58	59.94			
16/09/2024	60.50	60.58 (55.84–64.99)	0.83	60.50			
07/07/2025	60.20	60.29 (55.08–64.99)	0.92	60.20	56.96 (30.17–72.54)	6.69	58.32
03/10/2025	58.66	58.62 (55.80–59.42)	0.36	58.66	56.28 (20.15–75.13)	8.56	56.99
05/10/2025	59.33	59.26 (55.80–62.24)	0.49	59.33			
12/10/2025	59.25	59.21(55.87–62.13)	0.47	59.26			
13/10/2025	58.92	58.90(55.78–61.45)	0.34	58.93			

Table 5. In–situ measured water levels compared to estimated water levels using Sentinel-2 and Sentinel–1 estimates.

Water level (m)							
Date	In–situ water level (m)	Sentinel 2			Sentinel–1		
		Mean (Min–Max)	SD	Median	Mean (Min–Max)	SD	Median
23/02/2017	58.36						
24/02/2017	58.44	59.61 (43.95–75.50)	4.35	59.58	58.39 (21.58–108.21)	12.77	58.21
29/12/2019	58.98	63.28 (30.95–96.48)	7.75	61.78	59.37 (25.64–107.75)	14.53	59.09
30/12/2019	58.28				60.92 (12.71–108.25)	14.67	59.55
04/04/2022	59.94	59.13 (30.95–92.33)	6.87	59.23			
16/09/2024	60.50				62.08 (33.19–95.55)	8.62	60.92
07/07/2025	60.20	58.02 (31.44–68.87)	4.38	58.72	58.02 (31.44–68.87)	4.38	58.72
03/10/2025	58.66	58.45 (30.95–86.52)	5.83	58.91			
05/10/2025	59.33	57.73 (30.95–85.39)	5.56	58.29	59.97 (12.49–97.93)	8.19	59.95
12/10/2025	59.25	58.35 (30.95–102.75)	3.83	58.75			
13/10/2025	58.92	59.86 (33.19–105.56)	8.35	59.72			

Table 6. Water volumes calculated using the DEM and the different satellite products, and % difference (Diff.) between each satellite result and the reference DEM result.

Water volume (hm3)								
Date	In–situ water level (m)	DEM	Landsat 8/9	Diff.	Sentinel 2	Diff.	Sentinel–1	Diff.
23/02/2017	58.36	39.01	38.50	−1.3%				

24/02/2017	58.44	39.14			39.01	−0.3%	38.42	−1.9%
29/12/2019	58.98	40.06			39.76	−0.7%	38.29	−4.4%
30/12/2019	58.28	38.88	38.02	−2.2%			38.05	−2.1%
04/04/2022	59.94	41.70			41.45	−0.6%		
16/09/2024	60.50	42.69					41.73	−2.2%
07/07/2025	60.20	42.16	41.74	−1.0%	41.90	−0.6%	41.72	−1.0%
03/10/2025	58.66	39.51	38.87	−1.6%	39.28	−0.6%		
05/10/2025	59.33	40.65			40.27	−0.9%	40.19	−1.1%
12/10/2025	59.25	40.52			40.20	−0.8%		
13/10/2025	58.92	39.95			39.67	−0.7%		

Spatial variability exists along the shoreline based on DEM data, as demonstrated by the standard deviations of elevation (0.39–0.57 m), NDWI (0.06–0.20), and SAR backscatter (2.43–2.80 dB) in Table 2. This variability lends support to the hypothesis that the water's edge is formed from a transition zone rather than an abrupt discontinuity. The correspondence between the mean NDWI thresholds derived from the shoreline itself (–0.20 for Sentinel-2; –0.13 for Landsat) and those determined from the reservoir profiles is shown in Figure 5. With respect to the performance of the sensors, the markedly narrower NDWI range recorded by Landsat (SD 0.06–0.10) in comparison to Sentinel-2 (SD 0.17–0.20) can be attributed to the lower spatial resolution of the former. By averaging the spectral response of water and adjacent land surfaces over a larger area of land (900 m² vs. 100 m²), Landsat inherently reduces apparent radiometric fluctuations at the water's edge, resulting in excessive smoothing of the natural transition.

A comparative analysis of SAR (Sentinel–1) and multispectral (Sentinel-2 and Landsat 8/9) products reveals fundamental differences in their sensitivity for water detection, particularly when distinguishing between area and volume estimates. The most notable discrepancy was observed in the estimates of water–covered area (Table 3), which exhibited substantial variability between sensors (differences ranging from –6.0% to +8.0% relative to the DEM reference) and minimal correlation with measured water levels. This area of instability stands in marked contrast to the volume estimates presented in Table 6 and Figure 11, where all satellite–derived volumes consistently remained below the DEM reference (ranging from –0.3% to –4.4%) and showed near–perfect linear relationships with water level (R^2 close to 1 for NDWI–based methods). This paradoxical behaviour can be attributed to the hypsometric properties of the reservoir basin: while marginal transition zones introduce classification uncertainties that disproportionately affect planimetric area calculations, volumetric integration inherently smooths out these local discrepancies, as the central deep–water areas are reliably captured by both sensors.

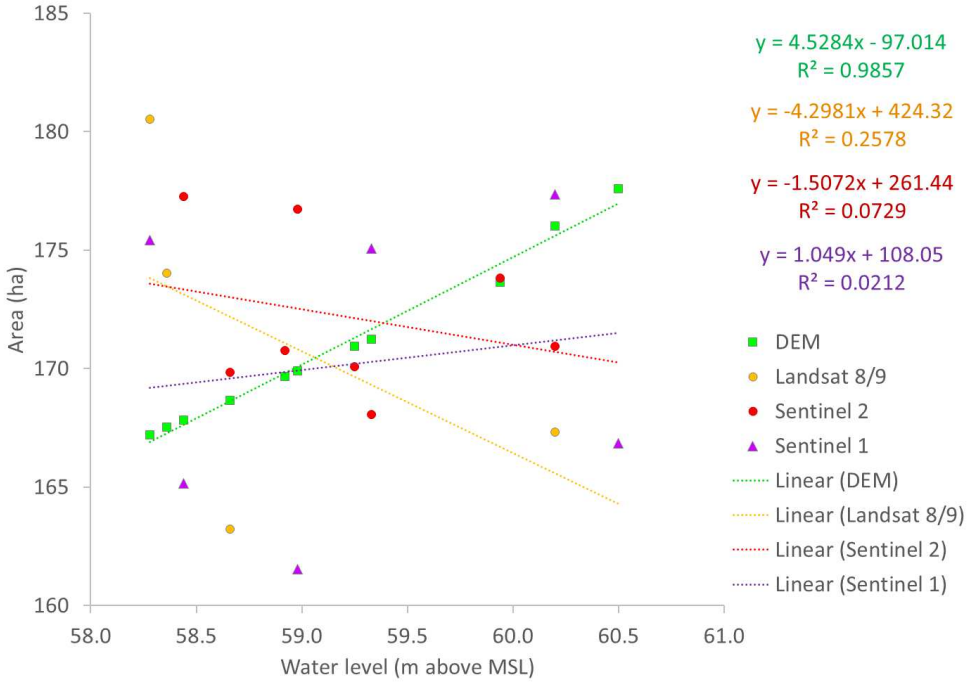


Figure 9. Water surface areas estimated using the DEM, Landsat 8/9 and Sentinel 2 satellite NDWI and Sentinel–1 Sigma, and respective linear trend lines.

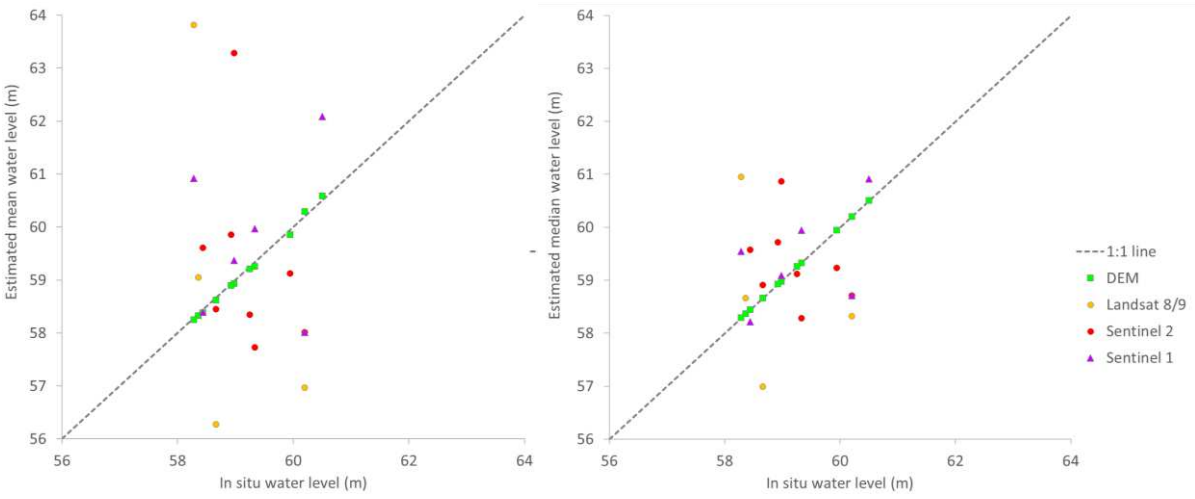


Figure 10. Mean (left) and median (right) water levels estimated using the DEM, Landsat 8/9 and Sentinel 2 satellite NDWI, and Sentinel–1 Sigma; the 1:1 line indicates perfect correlation.

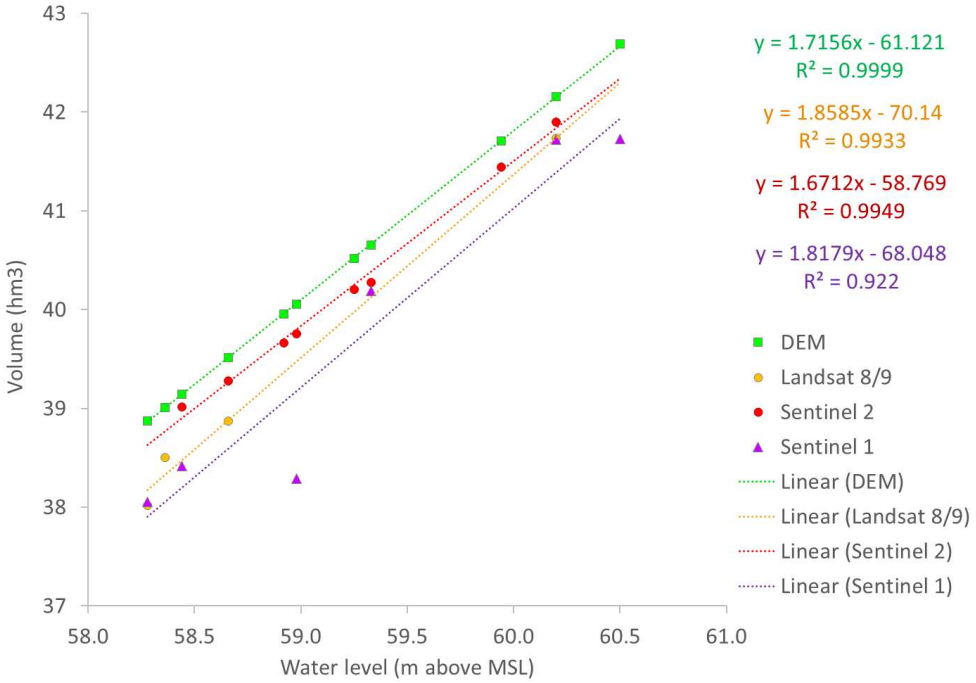


Figure 11. Water volumes estimated using the DEM, Landsat 8/9 and Sentinel 2 satellite NDWI and Sentinel–1 Sigma, and respective linear trend lines.

DISCUSSION

The integration of satellite–derived water extents with digital elevation model (DEM) data constitutes a widely adopted methodological framework for estimating reservoir storage dynamics without relying solely on in–situ measurements (Chen et al. 2024). Within this approach, the initial step entails the delineation of the water surface area from satellite imagery. Subsequently, the volume is calculated by intersecting this delineated area with the topographic information provided by the DEM. The reliability of this methodology depends on the implementation of appropriate sensor–specific calibration, as evidenced by the threshold values established in this study. The upper NDWI thresholds of –0.20 for Sentinel-2 and –0.13 for Landsat 8/9 reflect the inherent differences in spectral resolution and radiometric sensitivity between these optical sensors. However, both values remain consistent with previously reported ranges (Pena–Regueiro et al. 2023). Similarly, the Sentinel–1's –14 dB SAR backscatter threshold (VV polarization) aligns well with successful flood mapping applications, where thresholds between –12 and –16 dB are commonly used (Atchyuth et al. 2023).

Regarding sensor performance, estimates based on the normalized longwave width index (NDWI) from Sentinel-2 and Landsat consistently outperformed synthetic aperture radar (SAR)–derived Sigma values (R^2 = 0.922). This superior accuracy is physically based on the spectral response of water, as optical indices directly exploit the strong absorption of shortwave infrared (SWIR) and near–infrared (NIR) radiation by pure water, enabling accurate detection under clear sky conditions (McFeeters 1996). In contrast, SAR backscatter relies on the dielectric contrast between water and land, but its signal is critically modulated by surface roughness. As observed in the cross–sections (Figures 6e and 6f), the October SAR backscatter over the reservoir increased from –20 dB to between –12 and –14 dB. This increase is attributed to the enhanced surface roughness induced by the exposure of thicker substrates due to the decline in water level. This increase in roughness has been shown to result in an enhancement of the backscatter coefficient, leading to a partial masking of the reflection that is characteristic of still water bodies. This phenomenon occasionally results in misclassification of water pixels as land, thereby explaining the modest reduction in volumetric accuracy.

The marginal discrepancies observed in the water masks (Figure 8) further illustrate the distinct physical challenges faced by each technology. In the context of SAR, the presence of emergent aquatic vegetation has been observed to result in the generation of variable values, which, in turn, have been shown to yield double–bounce scattering effects (Brisco et al. 2013). These effects have been found to artificially augment backscatter, thereby leading to the under–detection of water edges. In the case of multispectral sensors, the spatial resolution (10–30 m) inherently generates mixed pixels at the land–water interface, where the subpixel fractions of water and land surfaces produce intermediate NDWI values close to the established thresholds (–0.20 for Sentinel-2 and –0.13 for Landsat), thus introducing areal uncertainties in the marginal areas.

The marked variability in water–covered areas estimated from different satellite sensors showed little correlation with the corresponding water levels (Table 3, Figure 9). This observation, whereby higher water levels do not consistently correspond to larger water areas, may be attributable to the geometric configuration of the reservoir basin. In reservoirs with steep bathymetric slopes, water-level fluctuations produce relatively small changes in surface area, whereas in flatter regions the same fluctuations can inundate extensive margins and therefore generate much larger changes in area (Pereira et al. 2019). Furthermore, temporal discrepancies between satellite overflights and in–situ water level measurements can introduce uncertainties, as water levels can fluctuate daily due to reservoir operational management. The disparities between satellite–derived areas and the digital elevation model (DEM) reference, ranging from –6.0% to +8.0% for all sensors, underscore that the selection of remote sensing method can exert a substantial influence on area estimates, thereby directly implicating water resource management decisions.

Furthermore, all satellite–based volume estimates demonstrated remarkable consistency with the DEM–derived reference volumes (Table 6, Figure 11), although they were consistently lower, with differences ranging from –4.4% to –0.3%. The observation that satellite–derived water masks tend to slightly underestimate the actual extent of water near the margins can be explained by two effects. Firstly, there is the presence of mixed–pixel effects (encompassing water and non–water areas). Secondly, there is the thresholding process.

The capacity of Sentinel–1 to acquire images under all weather conditions, both diurnally and nocturnally, ensures data continuity in regions frequently affected by cloud cover, where optical sensors would generate significant data gaps (Wagner et al. 2026). Consequently, while multispectral NDWI provides the highest accuracy for retrospective or cloud–free assessments, SAR is an indispensable complementary data source for operational reservoir monitoring under adverse weather conditions. The most robust strategy for ensuring reliable long–term hydrological monitoring is to integrate both datasets, rather than selecting a single optimal method.

Limitations and Future Perspectives

Several limitations of this study warrant acknowledgment. Firstly, the threshold selection was derived from a limited number of acquisition dates, which may not fully capture the seasonal and interannual variability of water conditions. Furthermore, environmental factors such as floating vegetation, algal blooms, and suspended sediments have been shown to significantly alter NDWI values and impede accurate water detection (Wang et al. 2018). Regarding SAR data, the exclusive use of VV polarization may not be optimal for all water detection scenarios. The incorporation of VH polarization or polarization ratios could provide complementary information, particularly for detecting water beneath vegetation (Brisco et al. 2013).

Furthermore, the Digital Elevation Model (DEM) used as a reference (Figure 6a) was assumed to remain static throughout the study period. Whilst this is a reasonable assumption for short–term reservoir bathymetry, it does not account for sedimentation processes that can alter the elevation–volume relationship over longer timescales, particularly in dynamic reservoir margins.

In order to address these limitations, long–term monitoring applications would benefit from periodic DEM updates or the integration of sediment transport models. Moreover, the incorporation of independent in–situ measurements across a broader range of water levels would serve to enhance the calibration process and thereby increase confidence in the resulting volume estimates.

Conclusions

Satellite–derived volume estimates demonstrated a high degree of consistency with DEM reference volumes, with differences ranging from –4.4% to –0.3%. Furthermore, NDWI–based volume–water level regressions yielded R^2 values approaching 1, indicating a strong linear relationship between estimated volume and water level.

In contrast to volume estimates, water surface area estimates exhibited higher variability across satellite products, ranging from –6.0% to 8.0% relative to the Digital Elevation Model (DEM). Consequently, the correlation between area estimates and measured water levels was notably poor.

A key finding of this study is the stark contrast between area–based and volume–based accuracy metrics: substantial discrepancies in shoreline delineation resulted in only minor differences in estimated storage volumes. This finding suggests that uncertainties in shoreline classification are partially mitigated during volumetric integration. Consequently, the practical impact of shoreline errors on reservoir storage assessment is likely to be lower than would be suggested by area–comparison metrics alone.

In conditions of clear–sky, optical indices have been shown to generally outperform Sentinel–1 SAR in terms of accuracy. Notwithstanding, SAR products remain indispensable for continuous monitoring, given their ability to acquire data irrespective of cloud cover and illumination conditions. This study contributes to the advancement of knowledge regarding the propagation of uncertainties from remote–sensing water masks to final storage estimates. By adopting this approach, a more decision–relevant framework is provided for the evaluation of the performance of reservoir monitoring methodologies.

References

Agência Portuguesa do Ambiente (2020) Cartas de zonas inundáveis a cartas de riscos de inundações. Agência Portuguesa do Ambiente

Agência Portuguesa do Ambiente (2025) Avaliação Preliminar dos Riscos de Inundações Região Hidrográfica – Douro 3.º Ciclo. Agencia Portuguesa do Ambiente

Atchyuth BAS, Swain R, Das P (2023) Near real-time flood inundation and hazard mapping of Baitarani River Basin using Google Earth Engine and SAR imagery. Environ Monit Assess 195:1331. https://doi.org/10.1007/s10661-023-11876-5

Brisco B, Schmitt A, Murnaghan K, et al (2013) SAR polarimetric change detection for flooded vegetation. Int J Digit Earth 6:103–114. https://doi.org/10.1080/17538947.2011.608813

Busker T, de Roo A, Gelati E, et al (2019) A global lake and reservoir volume analysis using a surface water dataset and satellite altimetry. Hydrol Earth Syst Sci 23:669–690. https://doi.org/10.5194/hess-23-669-2019

Chen Y, Wang Y, Li L, et al (2024) Monthly Monitoring of Inundated Areas and Water Storage Dynamics in China's Large Reservoirs Using Multisource Remote Sensing. https://doi.org/10.1029/2023WR036450

Crétaux J-F, Birkett C (2006) Lake studies from satellite radar altimetry. Comptes Rendus Géoscience 338:1098–1112. https://doi.org/10.1016/j.crte.2006.08.002

Cretaux J-F, Calmant S, Papa F, et al (2023) Inland Surface Waters Quantity Monitored from Remote Sensing. Surv Geophys 44:1519–1552. https://doi.org/10.1007/s10712-023-09803-x

Damkjaer S, Taylor R (2017) The measurement of water scarcity: Defining a meaningful indicator. Ambio 46:513–531. https://doi.org/10.1007/s13280-017-0912-z

Declaro A, Kanae S (2024) Enhancing Surface Water Monitoring through Multi-Satellite Data-Fusion of Landsat-8/9, Sentinel-2, and Sentinel-1 SAR. Remote Sens 16:3329. https://doi.org/10.3390/rs16173329

DGT (2026) Centro de Dados Geográficos da Direção-Geral do Território, Informação Territorial e LiDAR. In: Cent. Dados DGT. http://cdd.dgterritorio.gov.pt/dgt-fe/dgt-fe?language=pt. Accessed 26 Apr 2026

Donchyts G, Winsemius H, Baart F, et al (2022) High-resolution surface water dynamics in Earth's small and medium-sized reservoirs. Sci Rep 12:13776. https://doi.org/10.1038/s41598-022-17074-6

Dunmire D, Lievens H, Boeykens L, De Lannoy GJM (2024) A machine learning approach for estimating snow depth across the European Alps from Sentinel-1 imagery. Remote Sens Environ 314:114369. https://doi.org/10.1016/j.rse.2024.114369

Fikriyah VN, Darvishzadeh R, Laborte A, et al (2025) Temporal backscatter characterisation of ratoon rice crops based on Sentinel-1 intensity data. GIScience Remote Sens 62:2455081. https://doi.org/10.1080/15481603.2025.2455081

Filipponi F (2019) Sentinel-1 GRD Preprocessing Workflow. Proceedings 18:11. https://doi.org/10.3390/ECRS-3-06201

Goodman NR (1963) Statistical Analysis Based on a Certain Multivariate Complex Gaussian Distribution (An Introduction). Ann Math Stat 34:152–177. https://doi.org/10.1214/aoms/1177704250

Hou J, Van Dijk AIJM, Renzullo LJ, Larraondo PR (2024) GloLakes: water storage dynamics for 27 000 lakes globally from 1984 to present derived from satellite altimetry and optical imaging. Earth Syst Sci Data 16:201–218. https://doi.org/10.5194/essd-16-201-2024

Huang C, Chen Y, Zhang S, Wu J (2018) Detecting, Extracting, and Monitoring Surface Water From Space Using Optical Sensors: A Review. Rev Geophys 56:333–360. https://doi.org/10.1029/2018RG000598

Kossieris S, Tsiakos V, Tsimiklis G, Amditis A (2024) Inland Water Level Monitoring from Satellite Observations: A Scoping Review of Current Advances and Future Opportunities. Remote Sens 16:1181. https://doi.org/10.3390/rs16071181

Lekunberri X, David Ballester-Berman J, Arganda-Carreras I, Fernandes-Salvador JA (2024) Automatic mapping of aquaculture activity in the Atlantic Ocean. Int J Appl Earth Obs Geoinformation 132:104061. https://doi.org/10.1016/j.jag.2024.104061

Li Y, Gao H, Allen GH, Zhang Z (2021) Constructing Reservoir Area–Volume–Elevation Curve from TanDEM-X DEM Data. IEEE J Sel Top Appl Earth Obs Remote Sens 14:2249–2257. https://doi.org/10.1109/JSTARS.2021.3051103

McFeeters SK (1996) The use of the Normalized Difference Water Index (NDWI) in the delineation of open water features. Int J Remote Sens 17:1425–1432. https://doi.org/10.1080/01431169608948714

Musa ZN, Popescu I, Mynett A (2015) A review of applications of satellite SAR, optical, altimetry and DEM data for surface water modelling, mapping and parameter estimation. Hydrol Earth Syst Sci 19:3755–3769. https://doi.org/10.5194/hess-19-3755-2015

Pena-Regueiro J, Estornell J, Aguilar-Maldonado J, Sebastiá-Frasquet M-T (2023) Remote Sensing Temporal Reconstruction of the Flooded Area in "Tablas de Daimiel" Inland Wetland 2000–2021. Sensors 23:4096. https://doi.org/10.3390/s23084096

Pereira B, Medeiros P, Francke T, et al (2019) Assessment of the geometry and volumes of small surface water reservoirs by remote sensing in a semi-arid region with high reservoir density. Hydrol Sci J 64:66–79. https://doi.org/10.1080/02626667.2019.1566727

Rodell M, Famiglietti JS, Wiese DN, et al (2018) Emerging trends in global freshwater availability. Nature 557:651–659. https://doi.org/10.1038/s41586-018-0123-1

Roßberg T, Schmitt M (2025) Comparing the relationship between NDVI and SAR backscatter across different frequency bands in agricultural areas. Remote Sens Environ 319:114612. https://doi.org/10.1016/j.rse.2025.114612

Rossi D, Zolezzi G, Bertoldi W, Vitti A (2023) Monitoring Braided River-Bed Dynamics at the Sub-Event Time Scale Using Time Series of Sentinel-1 SAR Imagery. Remote Sens 15:3622. https://doi.org/10.3390/rs15143622

Scanlon BR, Fakhreddine S, Rateb A, et al (2023) Global water resources and the role of groundwater in a resilient water future. Nat Rev Earth Environ 4:87–101. https://doi.org/10.1038/s43017-022-00378-6

Schmidt K, Schwerdt M, Miranda N, Reimann J (2020) Radiometric Comparison within the Sentinel-1 SAR Constellation over a Wide Backscatter Range. Remote Sens 12:854. https://doi.org/10.3390/rs12050854

Schwatke C, Dettmering D, Bosch W, Seitz F (2015) DAHITI – an innovative approach for estimating water level time series over inland waters using multi-mission satellite altimetry. Hydrol Earth Syst Sci 19:4345–4364. https://doi.org/10.5194/hess-19-4345-2015

Schwatke C, Scherer D, Dettmering D (2019) Automated Extraction of Consistent Time-Variable Water Surfaces of Lakes and Reservoirs Based on Landsat and Sentinel-2. https://doi.org/https://doi.org/10.3390/rs11091010

Souza W, De Moura Reis LG, Ruiz-Armenteros AM, et al (2022) Analysis of Environmental and Atmospheric Influences in the Use of SAR and Optical Imagery from Sentinel-1, Landsat-8,

and Sentinel-2 in the Operational Monitoring of Reservoir Water Level. https://doi.org/https://doi.org/10.3390/rs14092218

Tedim F, Carvalho S (2010) Flood Management Strategies in Frequent and Small Scale Events: Lessons Learned from Amarante (Portugal). QUAGEO 29:69–84. https://doi.org/10.2478/v10117-010-0024-3

Tottrup C, Druce D, Meyer RP, et al (2022) Surface Water Dynamics from Space: A Round Robin Intercomparison of Using Optical and SAR High-Resolution Satellite Observations for Regional Surface Water Detection. Remote Sens 14:2410. https://doi.org/10.3390/rs14102410

Wagner W, Bauer-Marschallinger B, Roth F, et al (2026) The fully-automatic Sentinel-1 Global Flood Monitoring service: Scientific challenges and future directions. Remote Sens Environ 333:115108. https://doi.org/10.1016/j.rse.2025.115108

Wang J, Song C, Reager JT, et al (2018) Recent global decline in endorheic basin water storages. Nat Geosci 11:926–932. https://doi.org/10.1038/s41561-018-0265-7

Xu H (2006) Modification of normalised difference water index (NDWI) to enhance open water features in remotely sensed imagery. Int J Remote Sens 27:3025–3033. https://doi.org/10.1080/01431160600589179

Statements and Declarations

Funding

No funding was received for conducting this study.

Competing Interests:
The authors have no relevant financial or non–financial interests to disclose.

Data Availability:
The datasets generated during and/or analysed during the current study are available from the corresponding author on reasonable request.

Author Contributions:
All authors contributed to the study conception and design. Material preparation, data collection, and analysis were performed by I.C, A.M.B., M.C., and A.B. The first draft of the manuscript was written by I.C. and all authors commented on previous versions of the manuscript. All authors read and approved the final manuscript.

Ethics Approval
Not applicable. This study did not involve human participants or animals.

Acknowledgments
The authors thank FCT – Fundação para a Ciência e a Tecnologia, I.P., and the European Commission's Recovery and Resilience Facility for institutional support within the scope of projects UIDB/04423/2025 (https://doi.org/10.54499/UIDB/04423/2025), UID/PRR/04423/2025 (https://doi.org/10.54499/UID/PRR/04423/2025), and LA/P/0101/2020 (https://doi.org/10.54499/LA/P/0101/2020). A.M.B. also acknowledges the Scientific Employment Stimulus programme (2023.09258.CEECIND) of FCT for her research contract.